Optics Letters

# Photoacoustic-fluorescence microendoscopy *in vivo*

Wenzhao Yang,[1] Jiasheng Zhou,[1] Weihao Shao,[2] Myeongsu Seong,[1] Pengbo He,[1] Zhanhong Ye,[1] Zhendong Guo,[1] Lili Jing,[2] and Sung-Liang Chen[1,3,4,*]

[1]University of Michigan-Shanghai Jiao Tong University Joint Institute, Shanghai Jiao Tong University, Shanghai 200240, China
[2]School of Pharmacy, Shanghai Jiao Tong University, Shanghai 200240, China
[3]Engineering Research Center of Digital Medicine and Clinical Translation, Ministry of Education, Shanghai 200030, China
[4]State Key Laboratory of Advanced Optical Communication Systems and Networks, Shanghai Jiao Tong University, Shanghai 200240, China
*Corresponding author: sungliang.chen@sjtu.edu.cn

Received 22 March 2021; revised 5 April 2021; accepted 15 April 2021; posted 16 April 2021 (Doc. ID 425753); published 5 May 2021

**A miniature endoscope capable of imaging multiple tissue contrasts in high resolution is highly attractive, because it can provide complementary and detailed tissue information of internal organs. Here we present a photoacoustic (PA)-fluorescence (FL) endoscope for optical-resolution PA microscopy (PAM) and FL microscopy (FLM). The endoscope with a diameter of 2.8 mm achieves high lateral resolutions of 5.5 and 6.3 μm for PAM and FLM modes, respectively. *In vivo* imaging of zebrafish larvae and a mouse ear is conducted, and high-quality images are obtained. Additionally, *in vivo* endoscopic imaging of a rat rectum is demonstrated, showing the endoscopic imaging capability of our endoscope. By providing dual contrasts with high resolution, the endoscope may open up new opportunities for clinical endoscopic imaging applications.** 

https://doi.org/10.1364/OL.425753

Multimodal imaging is always desired as it provides complementary contrasts of tissue, thus being able to offer more complete characterization of tissue and more precise diagnosis of diseases. It is important to physically integrate different imaging modalities into a single unit in order to facilitate fast image acquisition, simple image co-registration, and even simultaneous monitoring of dynamic biological processes. Photoacoustic (PA) microscopy (PAM) is an emerging imaging modality capable of revealing optical absorption contrast in tissue with high spatial resolution [1]. It can noninvasively acquire anatomical, functional, and molecular characteristics of tissue. Fluorescence (FL) microscopy (FLM) can image fluorophores and has demonstrated a variety of biomedical applications [2]. By building a dual-modality PAM-FLM imaging system, co-registered microscopic images containing optical absorption and FL contrasts can be conveniently obtained, which is advantageous to offer more comprehensive insights into clinical diagnosis.

Since it is a valuable approach to acquire the two contrasts by PA and FL imaging, the dual-modality PAM-FLM imaging system has been the subject of several studies. To name a few, noninvasive mapping of sentinel lymph nodes *in vivo* was realized by PA and FL imaging [3]. Another example was using PA and FL imaging for *in vivo* imaging of tumor and ischemia mouse models [4]. In these works, individual PA and FL imaging systems were used separately [3,4]. A dual-modality imaging system integrating PAM and FLM was developed, and simultaneous angiography and lymphangiography were demonstrated [5]. A handheld probe capable of tri-modal imaging for SLN biopsy guidance was also reported [6]. Bulky imaging heads were employed in these integrated systems [5,6].

Medical endoscopes have been widely used for imaging applications such as gastrointestinal (GI) endoscopy [7–9]. In recent years, PA endoscopy, which is able to conduct PA imaging using miniature probes, has been explored by many groups [8,9]. Our lab has also demonstrated several miniature PAM probes with high resolution of the order of 1–10 μm [10,11]. Besides, FL endoscopy is a powerful tool for biomedical studies such as GI diseases [7]. If a miniature probe capable of PAM and FLM can be developed and used for endoscopy, it would allow the acquisition of both optical absorption and FL contrasts in an endoscopic manner. Further, it would facilitate clinical diagnosis because of one single endoscope used. Although a fiber-optic system for PAM and FLM using miniature components was demonstrated [12,13], the components were not assembled together and cannot be considered as fully developed for clinical use. An endoscope capable of both PAM and FLM with micrometer resolution using speckle illumination was presented [14]; yet no *in vivo* imaging was demonstrated, probably due to limited sensitivity and imaging speed. Development of a high-resolution PA-FL endoscope requires a decent design in order to optimize the imaging performance (e.g., high resolution and sufficient working distance [WD]) compared with a bulky PAM-FLM counterpart.

In this Letter, we report a PA-FL endoscope with a small diameter of 2.8 mm and high lateral resolution of 5.5 and 6.3 μm for optical-resolution PAM (OR-PAM) and FLM, respectively. We also conduct *in vivo* imaging of zebrafish larvae and a mouse ear using the endoscope. High resolution for both contrasts provided by the endoscope enables good image quality. More importantly, *in vivo* endoscopic imaging of a rat rectum is

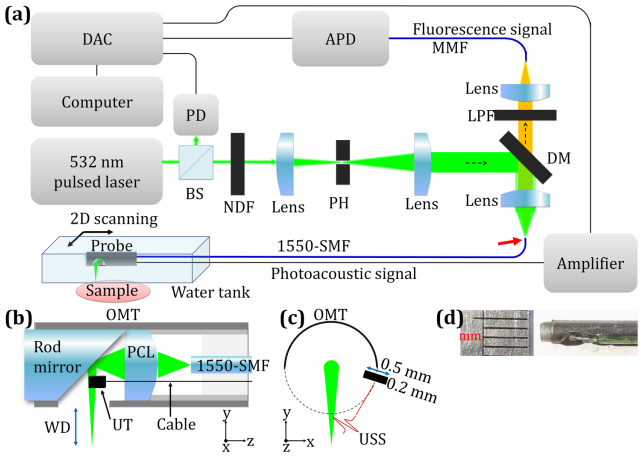


**Fig. 1.** (a) Schematic of the imaging experimental setup for the PA-FL endoscope. (b)–(d) Schematic and picture of the PA-FL endoscope: (b) Overall design, (c) cross-sectional view, and (d) picture. APD, avalanche photodiode; BS, beam splitter; DAC, data acquisition card; DM, dichroic mirror; LPF, long-pass filter; NDF, neutral density filter; PD, photodiode; PH, pinhole; PCL, plano-convex lens; USS, ultrasound signal; UT, ultrasonic transducer.

also demonstrated, showing the endoscopic imaging capability of our endoscope.

The schematic of the imaging experimental setup for our PA-FL endoscope is shown in Fig. 1(a). A 532 nm pulsed laser (FDSS532-Q4, CryLaS, Germany) with pulse duration of 2 ns and pulse repetition frequency (PRF) of 1 kHz was used as the excitation source for both PAM and FLM. The laser beam emitted from the laser head was first split into two beams by a 1:9 beam splitter (BS025, Thorlabs). One beam (10% power) was detected by a photodiode (DET10A2, Thorlabs) to provide triggers. The main beam (90% power) was first attenuated by neutral density filters and then passed through a beam shaping set, consisting of two plano-convex lenses and a pinhole, to produce a collimated beam with an enlarged beam diameter. After that, the beam was reflected by a dichroic mirror (DMLP550, Thorlabs) and finally coupled into a 1550 nm single-mode optical fiber (1550-SMF, core diameter: 9 μm, SMF-28e, Corning) via a doublet lens (AC127-030-A-ML, Thorlabs). Note that the doublet lens was chosen to match the numerical aperture (NA) of the 1550-SMF so as to optimize the coupling efficiency, and a fiber coupler (not shown) (F-915, Newport) was used to facilitate the laser coupling procedure.

For two-dimensional (2D) linear scanning [Fig. 1(a)], the endoscope (detailed design described later) was mounted on a 2D linear motorized stage (not shown) (M-404, Physik Instrumente, Karlsruhe, Germany) while, for rotary scanning in endoscopic imaging, the endoscope was mounted on a home-built belt-driven rotary scanning system (not shown), similar to the system reported in [15]. For easy illustration, 2D linear scanning is taken as an example in Fig. 1(a). Note that a window was opened in the bottom of the water tank and sealed with a thin plastic wrap (not shown) mainly to facilitate acoustic coupling for the PAM mode. For PAM, the laser was focused on a sample, and excited PA signals were detected by an ultrasonic transducer (0.6 mm × 0.5 mm × 0.2 mm; central frequency: 40 MHz; AT23730, Blatek), which was attached on the sidewall of the endoscope. A preamplifier (ZFL-500LN-BNC+, Mini-Circuits) was used to increase PA signal amplitudes. On the other hand, for FLM, the same focused laser was used to illuminate the sample, and induced FL signals were first collected by the endoscope and then transmitted backward by the 1550-SMF. The dichroic mirror and a long-pass filter (FELP0550, Thorlabs) were followed to suppress undesired 532 nm laser light (background) mainly due to reflection. Note that the coupling side (i.e., the red arrow in Fig. 1) of the 1550-SMF was angle polished so that the background laser light, due to the reflection there, can be well suppressed even before passing through the dichroic mirror and the long-pass filter. With the above arrangements, high signal-to-background ratios for FLM can be secured. Finally, FL signals were coupled into a multi-mode fiber (MMF, core diameter: 400 μm, QP-400-2-SR-BX, Ocean Optics) and detected by an avalanche photodiode (APD120A, Thorlabs). For both PAM and FLM, PA and FL signals were recorded by a data acquisition card (CSE1422, GaGe, Illinois) and stored in a computer.

A schematic and the picture of the PA-FL endoscope are shown in Figs. 1(b)–1(d). Figures 1(b) and 1(c) show the overall design and the cross-sectional view, respectively, of the endoscope. The endoscope consisted of the 1550-SMF (NA: 0.14), a plano-convex lens (diameter: 2 mm, 43-397, Edmund), and a rod mirror (diameter: 2 mm, 54-092, Edmund). The lens was for light focusing, and the rod mirror was for side-view imaging. The three components (the 1550-SMF, the lens, and the rod mirror) were coaxially aligned and fixed with three tubes [indicated by light- to dark-gray colors in Fig. 1(b)] by UV glue. The outermost metal tube (OMT) had an inner diameter of 2.1 mm and outer diameter of 2.5 mm. Note that a ∼180° side window [the dashed line in Fig. 1(c)] was opened around the distal end of the OMT to allow light and sound transmission. The WD, defined as the distance from the outer wall of the OMT to the laser focus, was measured to be ∼2 mm. The ultrasonic transducer was attached on the sidewall of the OMT. Owing to the side window of the OMT, the transducer can be placed with part of it inside the OMT [Fig. 1(c)], which is helpful to reduce the overall diameter of the endoscope. As shown in Fig. 1(d), the outer diameter of the endoscope is 2.8 mm.

Spatial resolution of the endoscope was measured. For the PAM mode, lateral resolution was measured by imaging the sharp edge of a razor blade. A detailed description of lateral resolution measured by using the sharp edge can be found in our previous work [16]. The lateral resolution of 5.5 μm was obtained. Axial resolution was measured by imaging a 6 μm carbon fiber. By checking the obtained PA A-line signal, axial resolution of ∼41 μm can be determined, which is mainly limited by the bandwidth of the transducer. On the other hand, for the FLM mode, lateral resolution was measured by imaging Rhodamine-B solution (concentration: $10^{-2}$ mol/L) with a blade used as a blocker for FL excitation. Specifically, the blade was attached below the plastic wrap at the bottom of the water tank [Fig. 1(a)], and the water tank was partially immersed in the Rhodamine-B solution. In this regard, the Rhodamine-B solution and water were isolated. Similarly, the sharp edge was imaged, and lateral resolution was measured to be 6.3 μm. Axial resolution was measured by imaging a thin layer (thickness: 25 μm) of the Rhodamine-B solution sandwiched between two transparent films. By moving the sample along the depth direction, the one-dimensional (1D) depth profile can be obtained (not shown). By checking the full width at half-maximum of the 1D depth profile, axial resolution of ∼110 μm was measured.

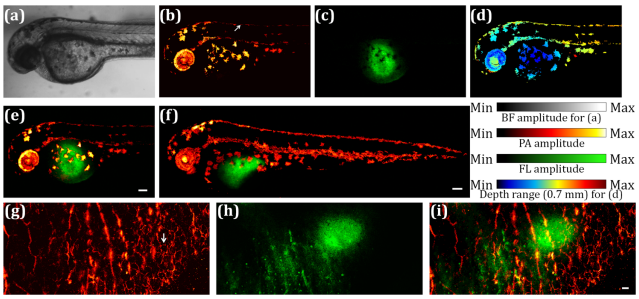


**Fig. 2.** (a)–(f) *In vivo* imaging of zebrafish larvae microinjected with a Rhodamine-B solution: (a) bright-field image, (b) PAM image (MAP), (c) FLM image, (d) PAM image (depth-encoded), (e) PAM-FLM fusion image [(b) and (c)], and (f) PAM-FLM fusion image of another zebrafish larva. (g)–(i) *In vivo* imaging of a mouse ear injected with a Rhodamine-B solution: (a) PAM image (MAP), (b) FLM image, and (c) PAM-FLM fusion image [(g) and (h)]. Scale bars: 100 μm. (a)–(e) share the same scale bar in (e). (g)–(i) share the same scale bar in (i). BF, bright-field.

To demonstrate *in vivo* imaging capability of the endoscope, imaging of zebrafish larvae and a mouse ear was performed. The results are shown in Fig. 2. 1.5 nL of the Rhodamine-B solution (concentration: $10^{-2}$ mol/L) was injected into the yolk sac by the PLI-90 injection device (Harvard apparatus). Detailed information of the zebrafish sample preparation can be found in our previous work [16]. A gray-scale bright-field image, as shown in Fig. 2(a), was first taken by using an optical microscope with a 5× objective and a charge-coupled device camera before imaging the zebrafish by the dual-modality endoscope. Then FLM was acquired by the endoscope, as shown in Fig. 2(c). Laser energy of 25 nJ/pulse was used. As can be seen, the FLM image displays strong FL signals at the region around the injection position (i.e., with sufficient Rhodamine-B) and no FL signals elsewhere. PAM was further acquired by scanning the endoscope over the same region of interest. To ensure high signal-to-noise ratios for the PAM image, higher laser energy of 150 nJ/pulse was used. Besides, a matched bandpass filter (30–60 MHz) and a local median filter were applied in post-processing. Figure 2(b) shows the PAM image in maximum amplitude projection (MAP). As can be seen, the detailed structure [e.g., small features as indicated by the arrow in Fig. 2(b)] is visualized, and different parts of the zebrafish (e.g., the eye, the yolk sac, and the body) can be identified. Note that the absorption contrast of zebrafish larvae is pigment. The pigment cells imaged here are mainly the epidermal melanophores (melanocytes). Figure 2(d) shows the depth-encoded PAM image (depth range: 0.7 mm) to demonstrate the three-dimensional imaging capability of the PAM mode. Finally, the PAM-FLM fusion image is shown in Fig. 2(e), where complementary contrasts can be better observed. It is worth mentioning that image co-registration can be done easily using the endoscope. Figure 2(f) shows the PAM-FLM fusion image of another zebrafish larva. The whole zebrafish was scanned. The image shows again the great imaging performance of the endoscope.

The probe was then used to image a mouse ear *in vivo*. Before imaging, ∼5 μL of the $10^{-2}$ mol/L Rhodamine-B solution was injected into the edge region of the mouse ear using a 30-gauge needle. Then imaging of lymphatic and blood vessels was performed immediately. The laser energy for FLM was 25 nJ/pulse, and that for PAM was 230 nJ/pulse. Figures 2(g)–2(i) show the PAM-FLM image. In the PAM image in Fig. 2(g), capillary beds were clearly resolved owing to the high resolution of our endoscope, and single capillaries [e.g., the one indicated by the arrow in Fig. 2(g)] were successfully imaged. In the FLM image in Fig. 2(h), FL signals appeared not only around the injection position but also elsewhere, which is evidence that Rhodamine-B molecules were circulated into lymphatic vessels. The fusion image in Fig. 2(i) demonstrates complementary contrasts obtained by dual-modality imaging. The high resolution would be advantageous in medical applications such as studying cancer metastasis in lymphatic and blood capillaries.

To further demonstrate the endoscopic imaging capability of the endoscope, *in vivo* endoscopic imaging of a rat rectum was conducted. For *in vivo* endoscopic imaging, another 532 nm pulsed laser (AO-S-532, cnilaser, China) operated at PRF of 4 kHz was used for improving the imaging speed. As mentioned previously, the belt-driven rotary scanning system was used to enable rotary scanning of the whole endoscope. The rotation was set to 1000 steps per 225° rotation, leading to a transverse step size of ∼13 μm, which is to balance the image quality and acquisition time. After each 225° rotation, the probe was pulled back by a motorized stage (M-404, Physik Instrumente, Karlsruhe, Germany), which completed 2D scanning. A male rat (SD, Shanghai SLAC Laboratory Animal Co., Ltd.) was used. Prior to image acquisition, the enema was applied to the rat, and then 2 ml Rhodamine-B dye solution ($5 \times 10^{-3}$ mol/L) was locally applied into the rectum from the anus to smear and stain the rectum tissue. During image acquisition, the rat was kept anesthetized. A steel tube (outer diameter: 6 mm) with a side window (180°), sealed with a thin plastic wrap [stretched to better follow the cylindrical shape of the steel tube, as shown in Figs. 3(a) and 3(b)], to facilitate side-view imaging was first inserted from the anus, and the endoscope was then inserted to acquire endoscopic images. Before inserting the steel tube, ultrasound gel was smeared over the outer surface of the steel tube to facilitate acoustic coupling, as well as easy insertion into the rat rectum. The rectum tissue was well attached around the outer boundary of the steel tube. Additionally, water was further filled in the steel tube to enable acoustic coupling. The plastic wrap was used to avoid water leakage and to enable light and sound transmission. The endoscope was coaxially aligned with the steel tube so that the scanning arc can well follow the boundary of the plastic wrap (i.e., tissue surface), as shown in Figs. 3(a) and 3(b). During image acquisition, the endoscope was rotated and pulled back, while the steel tube was kept stationary. In the future, to enable 360° rotation for endoscopic imaging, the endoscope can be further capped with a steel tube (having a small side window) so that the endoscope, together with the steel tube, can be rotated by 360° without any obstruction. As shown in Fig. 3, PAM and FLM images can visualize blood vessels and the Rhodamine-B-stained region of the inner surface of the rectum, respectively. Figures 3(c)–3(e) are for better displaying the vessel and dye distribution over the rat rectum. A vessel diameter down to ∼20 μm is identified [indicated by the arrows in Figs. 3(c) and 3(f)], showing the high-resolution capability of the endoscope. All experimental animal procedures were carried out in conformity with the laboratory animal protocol approved by the Laboratory Animal Care Committee of Shanghai Jiao Tong University.

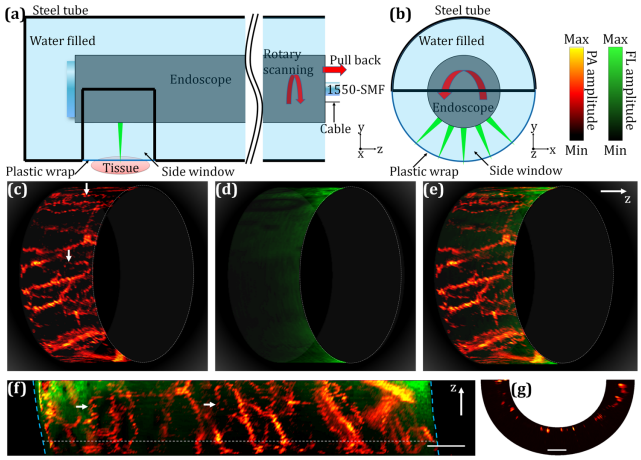


**Fig. 3.** *In vivo* endoscopic imaging of a rat rectum. (a) Schematic of the endoscope and the steel tube. (b) cross-sectional view of (a). (c) PAM image, (d) FLM image, and (e) PAM-FLM fusion image [(c) and (d)]. (c)–(e) displayed in cylindrical coordinate. (f) PAM-FLM fusion image [unfolded view of (e)]. The blue dashed line in (f) indicates the boundary of the side window, which spans 180°. (g) B-scan along the white dashed line in (f). Scale bars: 1 mm.

Currently, the 1550 nm SMF is used mainly because it has a larger core diameter to enable higher light coupling and collection efficiency for the FLM mode. By using a 532 nm SMF with a smaller core diameter of 2.5 μm (460-HP, Nufern), lateral resolution of both PAM and FLM can be further enhanced. In this case, one may employ a high-NA fiber to compensate for the decreased light coupling and collection efficiency. There is a trade-off between the resolution and depth of focus in microendoscopy. Focus-adjustable capability (e.g., using an optomechanical approach [11]) can be further developed in PA and/or FL microendoscopy to overcome the issue.

In Fig. 3, for PAM imaging, it took ∼0.26 min to acquire 800 PA A-lines (signal averaging of 32 times for each PA A-line) for a B-scan over the 180° window. For Fig. 3(c), we acquired 100 B-scans over 225° rotation to ensure covering the 180° window, which took approximately half an hour. On the other hand, because no signal averaging was applied for FLM imaging, it took ∼10 min to acquire Fig. 3(d). To improve the imaging speed for practical *in vivo* imaging, further development by adopting fiber-optic rotary joint assembly and "continuous-motion" (in contrast to "stop-and-go") scanning mechanism is needed [17].

The penetration depth of the OR-PAM mode and FLM mode is ∼1 mm and a few hundred microns, respectively [1,18]. Since a majority of cancers originate in the epithelial tissues of the human body, including those in the digestive system [19], the penetration depth is sufficient to study most GI cancers. In future, selected fluorescent dyes may be injected for endoscopic-related applications (e.g., indocyanine green to visualize lymphatic vessels for detection of sentinel nodes in intraoperative applications [20]).

In conclusion, a dual-modality PA-FL endoscope with a diameter of 2.8 mm was developed. High resolution for both PAM and FLM modes was achieved. Further, *in vivo* imaging of zebrafish larvae, a mouse ear, and a rat rectum (endoscopic imaging) was conducted to show the great imaging performance of the endoscope. Compared with similar works to develop PA-FL endoscopes [12–14,21–23], they have issues of incomplete assembly [12,13], low resolution (>100 μm) [22,23], or short WD (<100 μm) [14,21]. These issues might be the reasons why none of these works demonstrated *in vivo* endoscopic imaging.

**Funding.** National Natural Science Foundation of China (61775134).

**Disclosures.** The authors declare no conflicts of interest.

**Data Availability.** Data underlying the results presented in this paper are not publicly available at this time but may be obtained from the authors upon reasonable request.

## REFERENCES

1. L. V. Wang and S. Hu, Science **335**, 1458 (2012).
2. S. Nie, D. T. Chiu, and R. N. Zare, Science **266**, 1018 (1994).
3. Z. Liu, P. Rong, L. Yu, X. Zhang, C. Yang, F. Guo, Y. Zhao, K. Zhou, W. Wang, and W. Zeng, Mol. Pharm. **12**, 3119 (2015).
4. D. Peng, Y. Du, Y. Shi, D. Mao, X. Jia, H. Li, Y. Zhu, K. Wang, and J. Tian, Nanoscale **8**, 14480 (2016).
5. Y. Wang, K. Maslov, C. Kim, S. Hu, and L. V. Wang, IEEE Trans. Biomed. Eng. **57**, 2576 (2010).
6. J. Kang, J. H. Chang, S. M. Kim, H. J. Lee, H. Kim, B. C. Wilson, and T.-K. Song, Sci. Rep. **7**, 45008 (2017).
7. H. Stepp, R. Sroka, and R. Baumgartner, Endoscopy **30**, 379 (1998).
8. J. M. Yang, C. Favazza, R. Chen, J. Yao, X. Cai, K. Maslov, Q. Zhou, K. K. Shung, and L. V. Wang, Nat. Med. **18**, 1297 (2012).
9. K. Xiong, S. Yang, X. Li, and D. Xing, Opt. Lett. **43**, 1846 (2018).
10. G. Li, Z. Guo, and S.-L. Chen, IEEE Sens. J. **19**, 909 (2019).
11. Z. Guo, Z. Ye, W. Shao, L. Jing, and S.-L. Chen, "Miniature probe for optomechanical focus-adjustable optical-resolution photoacoustic endoscopy," arXiv:1911.09522 (2019).
12. P. Shao, W. Shi, P. Hajireza, and R. J. Zemp, J. Biomed. Opt. **17**, 076024 (2012).
13. S.-L. Chen, Z. Xie, L. J. Guo, and X. Wang, Photoacoustics **1**, 30 (2013).
14. A. M. Caravaca-Aguirre, S. Singh, S. Labouesse, M. V. Baratta, R. Piestun, and E. Bossy, APL Photonics **4**, 096103 (2019).
15. X. Li, K. Xiong, and S. Yang, Appl. Phys. Lett. **114**, 163703 (2019).
16. J. Zhou, W. Wang, L. Jing, and S.-L. Chen, Opt. Lett. **46**, 997 (2021).
17. J. Hui, Y. Cao, Y. Zhang, A. Kole, P. Wang, G. Yu, G. Eakins, M. Sturek, W. Chen, and J.-X. Cheng, Sci. Rep. **7**, 1417 (2017).
18. F. Leblond, S. C. Davis, P. A. Valdés, and B. W. Pogue, J. Photochem. Photobiol. B **98**, 77 (2010).
19. S.-L. Chen, Z. Xie, T. Ling, L. J. Guo, X. Wei, and X. Wang, Opt. Lett. **37**, 4263 (2012).
20. I. Miyashiro, K. Kishi, M. Yano, K. Tanaka, M. Motoori, M. Ohue, H. Ohigashi, A. Takenaka, Y. Tomita, and O. Ishikawa, Surg. Endosc. **25**, 1672 (2011).
21. S. Mezil, A. M. Caravaca-Aguirre, E. Z. Zhang, P. Moreau, I. Wang, P. C. Beard, and E. Bossy, Biomed. Opt. Express **11**, 5717 (2020).
22. C. Miranda, E. Marschall, B. Browning, and B. S. Smith, Photoacoustics **19**, 100167 (2020).
23. K. Zhan, L. Wang, Z. Chen, and D. Xing, IEEE J. Sel. Top. Quantum Electron. **27**, 7100105 (2021).